Integrated sub-terahertz waveguide reconfigurable attenuator based on Ge₂Sb₂Te₅ phase-change material

```
© S.V. Seliverstov<sup>1,2,7</sup>, A.K. Kozhukhovsky<sup>1</sup>, D.G. Fudin<sup>1</sup>, S.S. Svyatodukh<sup>1,3</sup>, P.I. Lazarenko<sup>4</sup>, D.Yu. Terekhov<sup>4</sup>, A.I. Prokhodtsov<sup>2</sup>, A.A. Nevzorov<sup>2</sup>, V.V. Svetukhin<sup>5</sup>, V.V. Kovalyuk<sup>2,3</sup>, G.N. Goltsman<sup>3,6</sup>
```

University of Science and Technology MISIS,

115419 Moscow, Russia

109028 Moscow, Russia

124498 Moscow, Russia

124498 Moscow, Russia

Russian Quantum Center "Skolkovo",

143026 Moscow, Russia

123458 Moscow, Russia

E-mail: sv.seliverstov@mpgu.su

Received March 26, 2025 Revised June 23, 2025 Accepted June 23, 2025

The use of chalcogenide semiconductor compounds, in particular the Ge-Sb-Te (GST) material with phase memory, is of great importance for the further development of terahertz (THz) micro- and nanoelectronics, including the creation of spatiotemporal THz modulators for high-speed wireless communications, elements of neuromorphic photonics, metamaterials for machine learning, as well as plasmonic devices and applications that provide data storage with the possibility of their subsequent reconfiguration. In this paper, we study the change in the signal passing through the THz waveguide depending on the phase state of the GST thin film covering the waveguide. In this work, two versions of waveguides were manufactured: unclad and based on an effective medium. The phase memory material was used to control the parameters of the transmitted signal. During the experiments it was found that the value of the absorption contrast between the amorphous and crystalline states of GST exceeds 10 dB for the case when the orientation of the electric field vector of the wave propagating along the waveguide is perpendicular to the GST layer. The obtained results open up the possibility of using the developed elements as reconfigurable attenuators in the creation of integrated THz photonics devices.

Keywords: chalcogenide semiconductors, phase-change material GST, terahertz photonics, high- resistivity silicon.

DOI: 10.61011/SC.2025.02.61364.7743

1. Introduction

The first quarter of the 21st century was marked by a growing need to increase the speed of wireless data transmission because of advances in areas such as high-resolution video streaming, the Internet of Things, augmented reality, and artificial intelligence (AI). The development of next-generation (6G) data transmission technologies in the terahertz (THz) and subterahertz (subTHz) bands is one of the solutions for this problem. An increase in the data transfer rate will be achieved in this case by increasing the frequency of the carrier signal. The use of AI capabilities in this case will further improve speed and quality by reducing transmission errors, identifying signs of real events from recorded signals, and redistributing hardware power in

real time to optimize traffic and computing. The potential of using AI for wireless communication has been demonstrated in practice [1]. In particular, solving the channel evaluation problem has made it possible to increase the efficiency of data transmission in communication systems of the current and previous generations. The solution to this problem is even more relevant for 6G systems, since THz radiation, which will be used in these systems, is strongly absorbed in the atmosphere by water vapor and therefore will have a high directivity. It is worth noting that the existing deterministic channel estimation algorithms cease to be effective when optimization is carried out using a large number of non-linearly related parameters. In this case, the use of AI capabilities is more than justified [2].

¹ Moscow Pedagogical State University,

¹¹⁹⁹⁹¹ Moscow, Russia

² Laboratory of Photonic Gas Sensors,

³ National Research University "Higher School of Economics",

⁴ "National Research University of Electronic Technology",

⁵ Scientific Manufacturing Complex "Technological Center",

⁶ Quantum Photonic Integrated Circuits Group,

⁷ Telecommunications R&D Institute, MIEM,

Similar AI-based systems have already been demonstrated In particular, methods based on the use of artificial neural networks (ANN) have already shown excellent performance in various wireless communication tasks, such as active user detection (AUD), spectrum sensing, and resource allocation [4,5]. In addition, attempts are being made to use machine learning (ML) to solve the problem of finding and evaluating a wireless channel in millimeter (MM) and THz systems with multiple inputs and multiple outputs (MIMO), as well as in the V2X (Vehicle-to-Everytning) system [6]. In response to this trend, the consortium developing specifications for 3GPP mobile telephony has included AI as one of the main components in 5G Advanced systems [7].

However, the previously proposed solutions were based on the use of classical computer architecture to implement ANN operation or on the basis of photonic integrated circuits (PIC) of the optical band. The first case has disadvantages associated with inefficiency and high energy consumption. The second implementation is related to the need to convert the THz signal into optical radiation to implement neuromorphic computing, and then reverse the conversion from optical to THz band. This significantly complicates the finished device, reduces its performance, and also increases the final cost.

Switching to the optical band is not needed in the case of 6G applications, since operation is possible exclusively in the THz region. Thus, the study of the possibilities of using THz integrated circuits for the physical implementation of neuromorphic computing in 6G communication systems is an urgent scientific task, because it is associated with the study of physical mechanisms that can be used for the hardware implementation of future THz ANN based on integrated waveguide circuits.

The basic operation required for the ANN operation is the scalar product of two vectors. The implementation of this operation using classical electronic devices (transistor chips) is associated with high power consumption. In the optical band, it is shown that a photonic chip performing the scalar product operation of vectors consumes a minimum amount of energy. The THz band is an equally promising candidate in this regard. The use of ANN implemented in hardware based on THz integrated photonic circuits will allow performing the required calculations "on the fly" with virtually no energy consumption, as well as without the need to store intermediate calculation results (so-called "fog calculations") [8]. At the same time, calculations will be performed within the THz band, without the need to convert to optical and vice versa, which will significantly simplify the finished device and reduce its final cost.

The use of AI systems based on classical computer architecture to solve the problem of channel search and evaluation has been successfully demonstrated in current and previous generations of wireless communication systems [2]. The implementation of neuromorphic computing based on optical PIC is also widely represented in the literature [9].

The scalar product involves the use of two arithmetic operations: addition and multiplication. Theoretically, it is shown that the implementation of these operations can be achieved using two active elements in a photonic circuit, namely an attenuator and a phase shifter [10]. In this case, the attenuator can be implemented by using a Mach-Zehnder interferometer, in one of the arms of which a phase shifter is integrated, and the phase of the signal at the output of the interferometer is adjusted by another phase shifter so that the signals at the output of each line of the computing chip are in-phase. A similar coherent implementation in the optical band has already been demonstrated earlier [11]. However, this approach is not always justified, as it complicates the final design. It is useful to have an attenuator in your arsenal as a separate basic integrated optical component.

The purpose of this study is to create a reconfigurable THz waveguide attenuator based on fully dielectric integral waveguide structures, in which attenuation is carried out by phase memory material Ge₂Sb₂Te₅ (GST).

Materials and methods

The use of chalcogenide semiconductor compounds, in particular GST material with phase memory, is important for the further development of THz micro- and nanoelectronics, including the creation of space-time THz modulators for high-speed wireless communications, elements of neuromorphic photonics, metamaterials for machine learning, as well as plasmonic devices and applications that provide data storage with the possibility of further reconfiguration [12]. Phase memory materials based on chalcogenide semiconductor compounds, in particular GST, are widely used in integrated photonics operating in the C-band $(\sim 1.55 \,\mu\text{m})$ [13]. The further development of science and industry provided by photonic integrated circuits is associated with progress in understanding the physics of these materials and their advancement to other parts of the electromagnetic spectrum. This is attributable to the unique properties of the GST material, which is able to switch between amorphous and crystalline states with significantly different optical and electrical properties. In this case, the state can be switched using a laser, simple heating, or electric current [14]. It is important that the acquired condition can be maintained for indefinite time at room temperature. The properties of GST in C-band, which is widely used in telecommunication applications, have been studied in detail.

The THz band is even more attractive in this regard. Recently, this band has attracted an increased attention among researchers and developers around the world due to the need to use it for development of applications related to next-generation data transmission systems in the THz (6G) band with ultra-high data transfer rates. It should be noted that the physics of GST operation in the THz band differs from that in the C-band, since the energy of THz quanta is

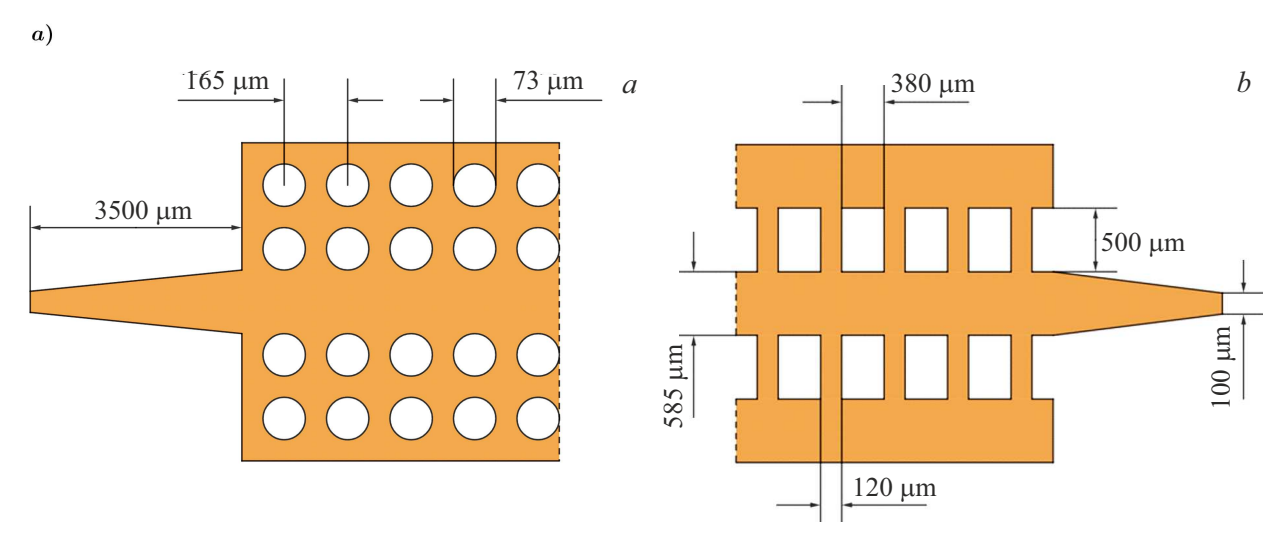


Figure 1. Geometry of the fabricated integral waveguide structures: a — waveguides with an effective medium; b — shell-free waveguides suspended on jumpers.

less than the energy gap of GTS, which is 0.7 and 0.4 eV in the amorphous and crystalline states, respectively [15]. Because of this, in particular, the contrast in the absorption of the material in the THz band should be more pronounced in case of a change in the GST phase state than in the optical band, which is confirmed by previously published papers.

The potential of using GST in integrated THz photonics has already been demonstrated in practice [16]. The provided metamaterial allowed achieving ultrafast optical modulation of THz resonances with a configurable switching speed. The absorbing properties of GST in the THz band were also studied [13]. In particular, it was shown that the real and imaginary parts of the refractive index, as well as the dielectric constant, increase with the increase of the annealing temperature. Significant differences in the absorption and conductivity of GST material in the THz band were also found when switching between cubic and hexagonal crystalline phases, whereas the changes in these properties were significantly lower in case of switching between amorphous and cubic phases.

This study characterizes an integrated attenuator which includes a thin (170 nm thick) GST film applied on the surface of a fully dielectric THz waveguide made of high-resistance (resistivity > 3 kOhm·cm) silicon (Si) substrate with a thickness of $400\,\mu\text{m}$.

As part of the work, two versions of waveguides were manufactured: shell-free and based on an efficient medium. In the first variant, the waveguide core was etched from a high-resistance Si substrate and suspended on $100\,\mu m$ thick pins to the Si core. In the second variant, the waveguide core was formed by forming holes on both sides of it. The effective refractive index in the area of the holes was less than the Si refractive index. More details about this type of waveguide are provided in our previous publications [17,18]. The width of the waveguide core in both configurations was $585\,\mu m$, which corresponds to the wavelength of the

radiation in Si. The distance between the holes and their diameter were 165 and 73 mm, respectively. The dielectric waveguide was matched with a hollow metal waveguide using a cone with a length of 3.5 mm and a vertex width of $100\,\mu\text{m}$. The structural drawings of both configurations are shown in Figure 1.

A reverse wave lamp was used in the experiment as a radiation source providing operation in the range of 126.5–145.5 GHz. A Schottky diode was used as a detector. The GST state was transformed from amorphous to crystalline by heating. For this purpose, the samples were annealed at a temperature of 200 °C for 15 min in an argon stream on a Linkam HFS600E-PB4 temperature table.

The structures were manufactured in several stages. At the first stage, a photoresist was applied to the plates of monocrystalline high-resistance Si to create alignment marks. FP-2514 was chosen as a positive photoresist. At the next stage, the photolithography process was carried out on the MJB4 mask photolithography or MLA100 mask-free photolithography installation, depending on the availability of the required photomask. After that, the substrates were immersed in a slightly alkaline solution of potassium hydroxide (KOH 0.8%) to develop the exposed photoresist. Then, the substrate with the developed photoresist was examined for defects using optical microscopy. absence of defects, the substrate was placed in an electron beam evaporation unit (Evatec BAK 501/800), where a thin layer of gold was applied to it through the windows in the photoresist. The substrate tagging stage was completed by rinsing the photoresist in warm acetone. Next, waveguide structures were formed. To do this, a chromium mask was applied to the Si surface, after which the topology of the waveguide structure was formed using photolithography. The Cr mask was etched into the photoresist windows, exposing the Si surface. Finally, Si was etched over the entire thickness of the substrate using deep reactive ion etching (Bosch process). The remains of the Cr mask were removed in a Cr liquid etchant.

Two types of experiments with straight waveguide sections were carried: with the excitation of wave modes with the direction of the electric field strength vector along \parallel and perpendicular \perp to the substrate plane. The desired mode was excited in the waveguide by using the necessary orientation of the rectangular waveguide relative to the dielectric waveguide (the wide side of the round metal waveguide was parallel to the substrate plane during perpendicular excitation and vice versa).

Modeling and experiment

First of all, we determined the length of the jumper, which ensures minimal propagation losses for suspended waveguides with the same width of $100\,\mu\text{m}$ using appropriate electromagnetic finite element modeling. The results obtained are shown in Figure 2.

It can be seen from the graphs that for all jumper lengths, the transmission coefficient of the waveguides increases with the increase of the frequency, but for waveguides with short jumpers, a sharper drop in transmission coefficient is observed at low frequencies. The transmission of both types of waveguides becomes approximately the same at the highest frequency. We attribute this to the fact that the radiation mode propagating through the waveguide becomes more localized in its core as the frequency increases. Therefore, the attenuating mode stops flowing into the Si banks, as it happens in waveguides with short jumpers at low frequencies, for which these banks are close to the core of the waveguide.

After determining the length of the jumpers $(500\,\mu\text{m})$ for the design of waveguides without a shell, we studied the transmission spectra of waveguides coated with thin films of GST material. GST films were sputtered on the surface of waveguide structures by magnetron sputtering of a polycrystalline target in a vacuum chamber. The technological details of the GST film sputtering process can be found in our previous publication [19]. The initial GST films were amorphous according to the data of Raman spectroscopy and X-ray diffraction. The thickness and surface roughness of the deposited GST films were $\sim 170\,\text{nm}$ and $< 1\,\text{nm}$, respectively.

Measurements were performed for two phases of GST (amorphous and crystalline) and for two polarizations. In the first case, the electric field strength vector in the exciting rectangular waveguide was directed perpendicular to the plane of the dielectric substrate of the waveguide, and it was parallel in the second case.

The results normalized for the transmission of a Si waveguide without a GST layer applied to it are shown in Figure 3. The obtained value of the transmission contrast between the two GST states exceeds 10 dB for the case of the orientation of the electric field vector propagating along the waveguide perpendicular to the GST layer. The

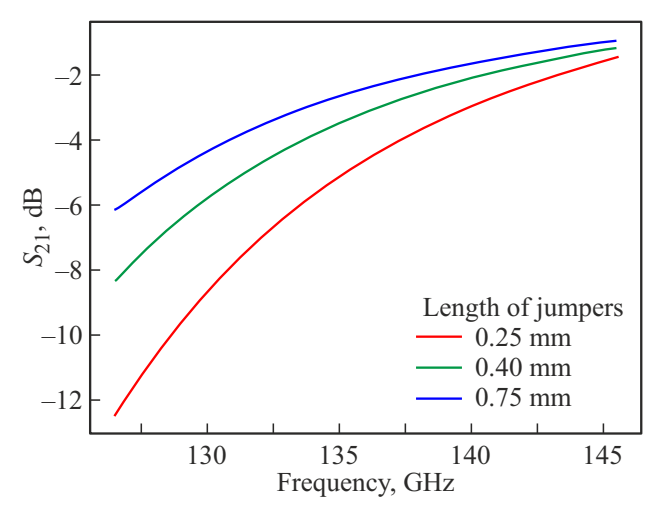


Figure 2. The results of modeling of the conductivity coefficients of shell-free integral waveguides at different lengths of the bridges suspending the waveguide core to the silicon backbone.

measured value of the return losses of waveguide structures with a GST layer sputtered on their surface in the crystalline state was $10.7 \, \mathrm{dB}$ at the emission frequency of $145.5 \, \mathrm{GHz}$. The obtained result suggests that the decrease in the transmission coefficient in case of the transition of the GST state from amorphous to crystalline is mainly determined by absorption rather than reflection. This absorption of THz radiation occurs on free carriers, the concentration of which significantly depends on the GST phase state [12]. It can be seen from the figure that the difference in absorption for two mutually perpendicular orientations of the vector E in the wave propagating through the waveguide is significant and amounts to $7.3 \, \mathrm{dB}$ at the emission frequency of $140 \, \mathrm{GHz}$.

This result is generally consistent with the results obtained in the optical band for similar structures. For example, it was previously shown that the effective refractive index of a dielectric waveguide optimized for 1.55 µm a wavelength with a thin GST layer on the surface of the waveguide depends on the phase state of the material [20]. the same time, there is also a significant difference in the spatial distribution of the wave field for two mutually perpendicular polarizations. For instance, the field is more concentrated near the surface of the waveguide in case of the GST crystalline state for the polarization of the E-vector perpendicular to the surface of the waveguide (E_{\perp} in our notation), which explains the stronger absorption in this case. Such a sharp "retraction" of the wave mode at $1.55 \,\mu\mathrm{m}$ wavelength in the GST layer is explained by the high value of the refractive index in the crystalline state.

The situation is significantly different in the THz band, since the wavelength is more than 3 orders of magnitude higher, and the GST layer is essentially two-dimensional. It is worth noting that the mechanism of GST absorption stated in previous publications is reduced to an increase in the concentration of free charge carriers during the transition

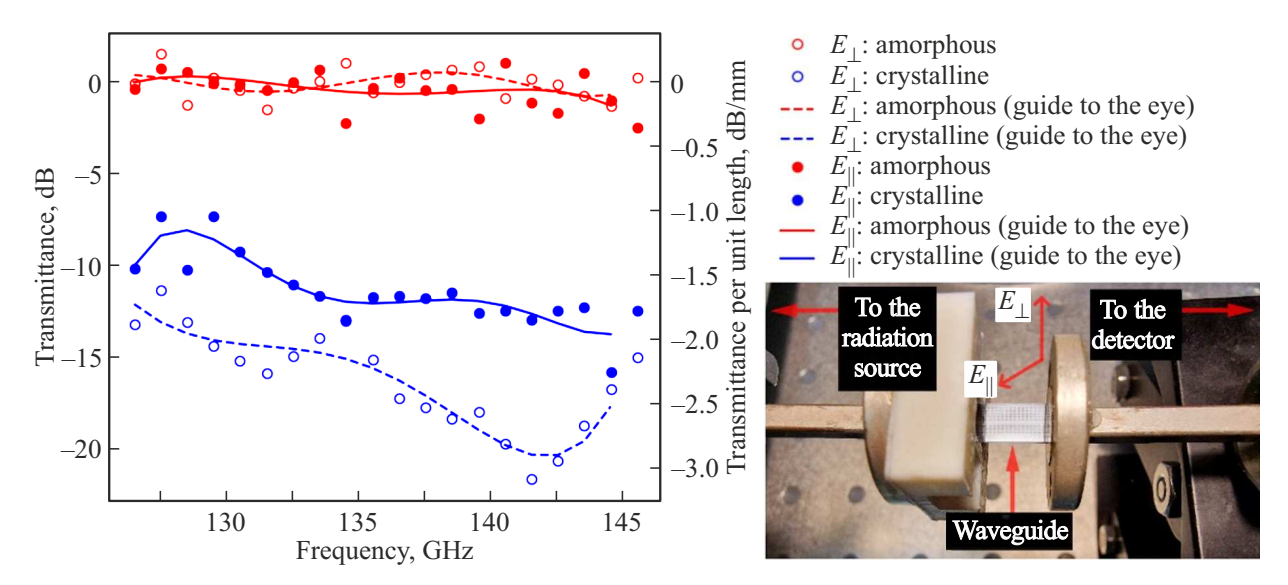


Figure 3. Transmission spectra of a silicon waveguide at different phase states of the GST surface layer and different radiation polarizations.

from an amorphous state to a crystalline one [12]. In this case, the difference in the absorption coefficient for two mutually perpendicular polarizations of the radiation passing through the waveguide is explained by the peculiarities of the spatial distribution of the wave mode with the polarization of the vector E perpendicular to the GST layer (TM mode), which is more concentrated on the upper and lower edges of the waveguide than in the case of oscillations of the vector E in a plane collinear to the plane of the GST layer (TE mode), which is more concentrated on the side surfaces of the waveguide, where there is no GST layer.

The results obtained confirm the possibility of using the studied structures in applications related to neuromorphic THz photonics. It is worth noting that there are many other phase memory materials besides GST. Various chalcogenide materials can be used as phase memory materials, for example, Sb₂Se₃, Sb₂S₃, GeTe, Ge-Sb-Se-Te, etc. However, compared to them, GST material has a number of advantages, including high writing and reading speed [21], high number of phase switching cycles without degradation of the material characteristics [22], good scalability and low power consumption [23], as well as the multi-level data storage capability [24]. These properties make GST particularly suitable for non-volatile memory applications.

4. Conclusion

In conclusion, we note that in the course of the work, a reconfigurable waveguide attenuator with a thin layer of GST applied to the surface of the waveguide core was developed and manufactured. The absorbing properties of a material with phase memory in the THz band in amorphous and crystalline states have been studied. Differences in the absorption coefficient for two different polarizations of THz radiation propagating through the waveguide are revealed.

The results obtained make it possible to significantly expand the capabilities of devices currently being created related to future THz communication systems, neuromorphic computing on THz integrated circuits, as well as plasmonic devices and data storage devices.

Funding

The study was supported by the Russian Science Foundation grant No. 20-79-10322, https://rscf.ru/project/20-79-10322/ (sputtering of GST films and their experimental study), the Ministry of Education and Science, the Ministry of Science and Higher Education of the Russian Federation (FSME-2025-0002) (fabrication of PIC), as well as within the framework of the HSE Fundamental Research Program (experimental study of transmission spectra of integral waveguides).

Conflict of interest

The authors declare that they have no conflict of interest.

References

- [1] T. Erpek, T.J. O'Shea, Y.E. Sagduyu, Y. Shi, T.C. Clancy. *Development and Analysis of Deep Learning Architectures*, 223 (2020).
- [2] W. Kim, Y. Ahn, J. Kim, B. Shim. B. J. Commun. Networks, 25 (1), 61 (2023).
- [3] W. Xia, S. Rangan, M. Mezzavilla, A. Lozano, G. Geraci, V. Semkin, G. Loianno. IEEE Trans. Wireless Commun., 21 (11), 9417 (2022).
- [4] H. Ju, S. Kim, Y. Kim, B. Shim. IEEE Trans. Wireless Commun., 21 (8), 6539 (2022).
- [5] K. Suh, S. Kim, Y. Ahn, S. Kim, H. Ju, B. Shim. IEEE Access, 10, 7384 (2022).

- [6] X. Ma, Z. Gao, F. Gao, M. Di Renzo. IEEE J. Select. Areas Commun., 39 (8), 2388 (2021).
- [7] A. Manoj, A.P. Kannu. IEEE Trans. Commun., 66 (11), 5678 (2018).
- [8] Resul Das, Muhammad Inuwa. Telematics and Informatics Rep., 10, 100049 (2023).
- [9] B.J. Shastri, A.N. Tait, T. Ferreira de Lima, W.H. Pernice, H. Bhaskaran, C.D. Wright, P.R. Prucnal. Nature Photonics, 15 (2), 102 (2021).
- [10] D.A. Miller. Optica, 2 (8), 747 (2015).
- [11] S. Xu, J. Wang, H. Shu, Z. Zhang, S. Yi, B. Bai, X. Wang, J. Liu, W. Zou. Light: Sci. Appl., 10 (1), 221 (2021).
- [12] K. Makino, K. Kato, Y. Saito, P. Fons, A.V. Kolobov, J. Tominaga, T. Nakano, M. Nakajima. J. Mater. Chem. C, 7 (27), 8209 (2019).
- [13] C. Ríos, M. Stegmaier, P. Hosseini, D. Wang, T. Scherer, C.D. Wright, H. Bhaskaran, W. Pernice. Nature Photonics, 9 (11), 725 (2015).
- [14] Y.G. Jeong, Y.M. Bahk, D.S. Kim. Adv. Optical Mater., 8 P.I.(3), 1900548 (2020).
- [15] P.I. Lazarenko, Y.V. Vorobyov, M.E. Fedyanina, A.A. Sher-chenkov, S.A. Kozyukhin, A.O. Yakubov, A.V. Kukin, Yu.S. Sybina, I.V. Sagunova. Inorganic Mater.: Appl. Res., 11, 330 (2020).
- [16] P. Pitchappa, A. Kumar, S. Prakash, H. Jani, T. Venkatesan, R. Singh. Advanced Mater., 31 (12), 1808157 (2019).
- [17] S. Seliverstov, S. Svyatodukh, G. Goltsman. Appl. Phys. Lett., 123 (9), 090501 (2023).
- [18] S. Seliverstov, A. Kozhukhovsky, S. Svyatodukh, G. Goltsman. Appl. Phys. Lett., 124 (12), 121106 (2024).
- [19] P. Lazarenko, V. Kovalyuk, P. An, A. Prokhodtsov, A. Golikov, A. Sherchenkov, S. Kozyukhin, I. Fradkin, G. Chulkova, G. Goltsman. APL Materials, 9 (12), 121104 (2021).
- [20] E. Menshikov, P. Lazarenko, V. Kovalyuk, S. Dubkov, N. Maslova, A. Prokhodtsov, A. Vorobyov, S. Kozyukhin, G. Goltsman, I.S. Sinev. ACS Appl. Mater. Interfaces, 16 (29), 38345 (2024).
- [21] P. Guo, A.M. Sarangan, I. Agha. Appl. Sci., 9 (3), 530 (2019).
- [22] D. Lawson, S. Blundell, M. Ebert, O.L. Muskens, I. Zeimpekis. Optical Mater. Express, 14 (1), 22 (2023).
- [23] W. Zhou, Z. Zhang, Q. Zhang, D. Qi, T. Xu, S. Dai, X. Shen. Micromachines, 12 (6), 616 (2021).
- [24] C. Zhang, M. Wei, J. Zheng, S. Liu, H. Cao, Y. Huang, Y. Tan, M. Zhang, Y. Xie, Z. Yu, J. Li, H. Ye, L. Li, H. Lin, H. Li, Y. Shi, L. Liu, D. Dai. Adv. Optical Mater., 11 (8), 2202748 (2023).

Translated by A.Akhtyamov